

Nanostructures made from superconducting boron doped diamond

Soumen Mandal[†] § , Cécile Naud[†] , Oliver A. Williams[‡] ,
Étienne Bustarret[†] , Franck Omnès[†] , Pierre Rodière[†] ,
Tristan Meunier[†] , Laurent Saminadayar[†] ¶ § and Christopher
Bäuerle[†] §

[†] Institut Néel, CNRS and Université Joseph Fourier, 38042 Grenoble, France

[‡] Fraunhofer Institut Angewandte Festkörperphysik, Tullastraße 72, 79108 Freiburg, Germany

¶ Institut Universitaire de France, 103 boulevard Saint-Michel, 75005 Paris, France

Abstract. We report on the transport properties of nanostructures made from boron-doped superconducting diamond. Starting from nanocrystalline superconducting boron-doped diamond thin films, grown by Chemical Vapor Deposition, we pattern by electron-beam lithography devices with dimensions in the nanometer range. We show that even for such small devices, the superconducting properties of the material are well preserved: for wires of width less than 100 *nm*, we measure critical temperatures in the Kelvin range and critical field in the Tesla range.

PACS numbers: 73.23.-b, 75.20.Hr, 72.70.+m, 73.20.Fz

1. Introduction

The discovery of superconductivity[1] in MgB_2 has generated a lot of interest for a special class of superconducting materials belonging to the covalent metals. In this context, the observation of superconductivity in highly-doped boron diamond[2] paved the way to the study of superhard superconducting materials[3, 4]. Apart from the fundamental point of understanding of the physical mechanisms leading to the superconductivity in these systems, their interest lies in a very high Young's modulus, which makes them promising candidates for the fabrication of superconducting Nano Electro-Mechanical Systems of exceptional quality factor. Evidences that *both* the superconductivity[5, 6, 7] *and* the mechanical properties[8] are essentially preserved in nanocrystalline layers grown on non-diamond substrates such as silicon have to be checked in order to bring further credit to this approach.

Most of the studies, however, have so far focused on the properties of *bulk* superconducting diamond, and it still remains to be shown what happens when the material is patterned into nanostructures. In this paper, we present a comprehensive study of nanostructured superconducting polycrystalline diamond films. Our measurements show that the critical temperature of the nanostructures being ≈ 2.5 K while for the bulk this is ≈ 3.5 K. The critical field for these structures is approximately 500mT at 50mK.

2. Experimental

The nanocrystalline boron-doped diamond was obtained by Chemical Vapour Deposition on a silicon oxide wafer. Prior to growth, wafers were cleaned with $NH_3OH : H_2O_2 : H_2O$ (1 : 1 : 5) solution at $75^\circ C$ for 10 *min*, and rinsed in pure DI water in an ultrasonic bath. In order to enhance nucleation, wafers were then seeded with diamond nanoparticles from an aqueous colloid of mono-disperse diamond particles known to have sizes less than 7 *nm* in solution as confirmed by dynamic light scattering[9, 10]. Atomic Force Microscope (AFM) measurements have shown this technique to result in uniform nucleation densities far in excess of $10^{11} cm^{-2}$. Diamond growth was then performed by microwave plasma enhanced chemical vapour deposition (MPCVD) from 4% CH_4 diluted in H_2 with additional boron from a trimethylboron gas source. The microwave power was 3000 *W* at 60 *mbar*, the substrate temperature being around $800^\circ C$ as monitored in situ with a bichromatic pyrometer.

Nanostructured devices have then been fabricated from this material. In figure 1 we present a diagram of the entire nanofabrication process. The wafer was first spin-coated with 4% polymethyl-methacrylate (PMMA) to form a 250 *nm* thick layer and prebaked at $180^\circ C$ for 5 *min*. The next step was the exposure to the electron beam with a dose of $360 \mu C \cdot cm^{-2}$ for an acceleration voltage of 20 *kV*. After exposure, the pattern was developed in 1 : 3 solution of methyl isobutyl ketone (MIBK) and iso-propyl alcohol (IPA) for 1 *min*. A thin layer of nickel (65 *nm*) has then been deposited and patterned

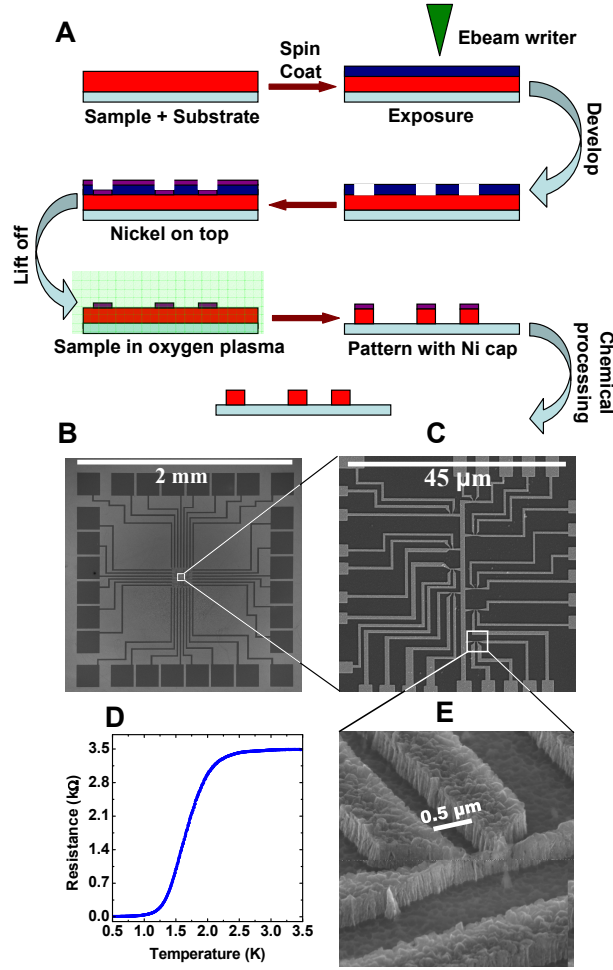


Figure 1. Schematics of the nanofabrication process with SEM images of a typical microcircuit. Panel B shows the SEM micrograph of the microcircuit used in our experiments. Panel C shows the magnified view of a $50 \times 50 \mu\text{m}^2$ area in the middle of the microcircuit. Panel E is the slanted view of the thinnest line we obtained which is 500 nm long, 90 nm wide and 300 nm high. The R vs T curve for this wire is shown in panel D: a clear superconducting transition is observed at $T \approx 1.7 \text{ K}$.

using a standard electron-gun evaporator and lift-off technique. This Ni layer acts as a mask for the plasma etching of the diamond structures subsequently done using Electron Cyclotron Resonance oxygen plasma[11] and a -27 V dc bias for $\approx 8 \text{ min}$. This leads to an etching rate of $\approx 40 \text{ nm/min}$. This mask was finally removed using an $FeCl_3$ solution. Ohmic contacts were then obtained by an evaporation of metals ($Ti - Au$).

Panel B, C and E of figure 1 show SEM pictures of the obtained nanostructures, namely wires of different widths and lengths. Panel E represents the smallest device we have been able to fabricate, a wire of length 500 nm and width 90 nm ; note that in this case the aspect ratio is as high as $\sim 1 : 3$, the anisotropy of the plasma etching allowing to pattern one single grain. The superconducting transition of this wire is presented in panel D showing a critical temperature of $\approx 1.7 \text{ K}$. Panel B in figure 1 shows a typical

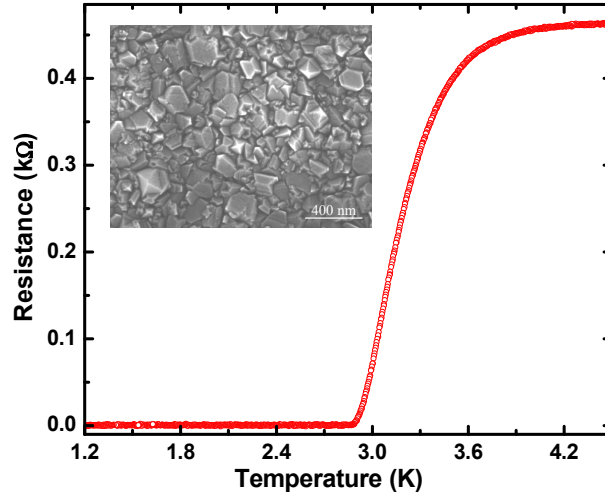


Figure 2. Superconducting resistive transition in a boron-doped diamond thin film. The inset is a Scanning Electron Microscope (SEM) image of the surface of the sample, consisting of grains of typically $\approx 150 \text{ nm}$.

microcircuit used for our measurements and panel C is the blow-up of a $50 \times 50 \mu\text{m}^2$ area in the center of the microcircuit.

3. Results and Discussion

A Scanning Electron Microscope (SEM) picture (inset of figure 2) of the sample shows grains of typical size $\approx 150 \text{ nm}$ for a film thickness of $\approx 250 \text{ nm}$, consistent with the nucleation density. Four silver paste electrical contacts, about 5 mm apart from each other, have been deposited at the surface for the characterisation of the as-grown layer. The 4-points resistance was measured as a function of temperature using these contacts and a standard *ac* lock-in technique under a very low current injection of $1 \mu\text{A}$. Typical data are presented in figure 2: a clear superconducting transition is observed with a zero resistance at $\approx 3 \text{ K}$. The width of the transition is quite large, typically 0.7 K with a 10 % – 90 % of the onset resistance criterion; we attribute this width to the distribution of the sizes of the grains in the material.

Electrical characterisation of the devices were performed in both a ^3He and a $^3\text{He}/^4\text{He}$ dilution refrigerators. Bottom panel of figure 3 shows the critical temperature T_c of wires of various widths, measured with very low current (typically 100 nA); no significant difference was observed from the critical temperature measured on the “bulk” sample ($\approx 2 \text{ K}$ for this wafer) except for the case of the narrowest wire (below 100 nm wide, $T_c \approx 1.7 \text{ K}$). This is a generic observation for all our samples: the critical temperature of our wires is those of the bulk material except for wires thinner than typically $\approx 100 \text{ nm}$; in this case, T_c it is slightly reduced. Figure 3 shows the voltage-current ($V - I$) characteristic of a 500 nm wide wire measured at different temperatures[12]. The $V - I$ curves are hysteretic due to thermal effect: when the critical

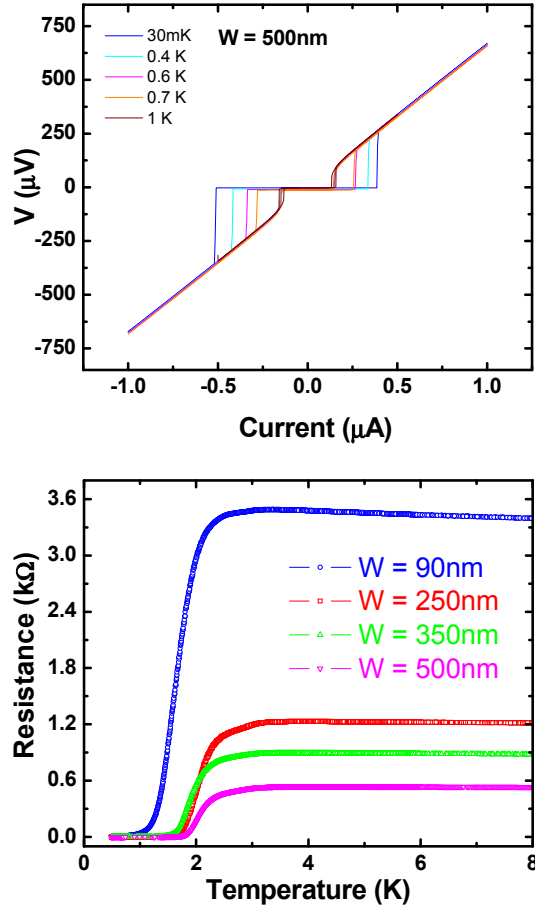


Figure 3. Voltage-current ($V - I$) characteristic of a 500 nm wide wire at different temperatures are shown in top panel. The $V - I$ curves are hysteretic due to thermal effect (Joule heating). The bottom panel shows the R vs T curves for four representative wires.

current is reached, Joule effect heats up the wire and the critical current measured when subsequently *decreasing* the current is thus much lower than the critical current measured when *increasing* the current[13, 14]; moreover, this “retrapping” current is independent of the temperature of the refrigerator, as the *actual* temperature of the sample is then fixed by the *dc* current trough the wire.

Critical field measurements were performed by applying a magnetic field perpendicular to the structure. $V - I$ characteristics for a 500 nm wide wire under different magnetic fields and at 50 mK are presented on the top panel of figure 4. As expected, the critical current decreases when applying a magnetic field. It should be stressed that for magnetic fields larger than 30 mT, the $V - I$ characteristic is not hysteretic: in this case, the Joule heating becomes negligible as the critical current is strongly lowered, and both (“*increasing*” and “*decreasing*”) critical currents become similar. In order to get more insights on the superconductivity of our devices under magnetic field, we have numerically calculated the derivatives of the $V - I$

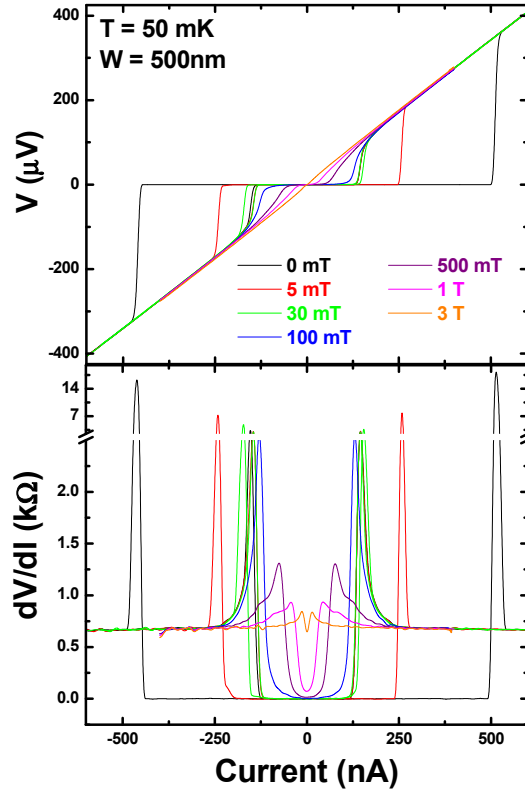


Figure 4. Voltage-current ($V - I$) characteristic of a 500 nm wide wire at 50 mK under different magnetic fields. The field is applied perpendicular to the plane of the sample. Only the “increasing” parts of the characteristics have been plotted. The behaviour is hysteretic until the applied field reaches 30 mT . The bottom panel shows the differential resistance extracted from the $V - I$ curves. The resistance goes to zero when the wire is in its superconducting state.

characteristics: the obtained $\frac{dV}{dI}(I)$ curves are displayed on the bottom panel of figure 4. For magnetic fields smaller than 500 mT , a clear zero is observed around $I = 0$, as expected for a superconductor. More interestingly, we observe a dip at zero current in the $\frac{dV}{dI}(I)$ characteristic for magnetic fields above 3 T . This demonstrates that one can still observe traces of superconductivity above 3 T in our nanometric wires, the most probable mechanism being that some grains remain superconducting under very high magnetic fields. More local studies, such as Scanning Tunneling Spectroscopy measurements[15, 16], are certainly desirable to fully understand the robustness of the superconductivity observed in our system.

4. Conclusion

In conclusion, we have successfully fabricated nanostructures from boron-doped nanocrystalline superconducting diamond. Using electron beam lithography, we have fabricated devices of characteristic size less than 100 nm and aspect ratio as high as $1 : 3$. These structures have critical temperatures in the Kelvin range, similar to

what is observed in “bulk” films; typical bulk T_c being 3.5K while for nanostructures it is 2.5K except for 90nm wire where it is ≈ 1 K. We measure critical fields close to 500 mT and traces of superconductivity are observed above 3 T. This study proves that superconductivity in boron-doped diamond is a very robust phenomenon which makes it a promising candidate for future applications in the field of superconducting Nano Electro-Mechanical Systems.

Acknowledgments

We thank L. Marty for help in the AFM measurements and P. Mohanty and M. Imboden for fruitful discussions. This work has been supported by the French National Agency (ANR) in the frame of its programme in “Nanosciences and Nanotechnologies” (SUPERNEMS project n° ANR – 08 – NANO – 033). O.A.W. acknowledges financial support from the Fraunhofer Attract award “Hybrid HF-MEMS Filters for GHz-Communication and capillary MEMS systems for chemical and biochemical Sensing - COMBIO”.

References

- [1] J. Nagamatsu, N. Nakagawa, T. Muranaka, Y. Zenitani and J. Akimitsu, *Nature* **410**, 63 (2001).
- [2] E. A. Ekimov, V. A. Sidorov, E. D. Bauer, N. N. Mel'nik, N. J. Curro, J. D. Thompson and S. M. Stishov, *Nature* **428**, 542 (2004).
- [3] X. Blase, É. Bustarret, C. Chapelier, T. Klein and C. Marcenat, *Nature Materials* **8**, 375 (2009).
- [4] G. A. Dubitskiy, V. D. Blank, S. G. Buga, E. E. Semenova, V. A. Kulbachinskii, A. V. Krechetov and V. G. Kytin, *JETP Lett.* **81**, 260 (2005)
- [5] M. Nesládek, D. Tromson, C. Mer, P. Bergonzo, P. Hubik and J. J. Mares, *Appl. Phys. Lett.* **88**, 234111 (2006).
- [6] W. Gajewski, P. Achatz, O. A. Williams, K. Haenen, È. Bustarret, M. Stutzmann and J. A. Garrido, *Phys. Rev. B* **79**, 045206 (2009).
- [7] P. Achatz, W. Gajewski, É. Bustarret, C. Marcenat, R. Piquerel, C. Chapelier, T. Dubouchet, O. A. Williams, K. Haenen, J. A. Garrido and M. Stutzmann, *Phys. Rev. B* **79**, 201203 (2009).
- [8] M. Imboden, P. Mohanty, A. Gaidarzhy, J. Rankin and B. W. Sheldon, *Appl. Phys. Lett.* **90**, 173502 (2007).
- [9] O. A. Williams, O. Douhéret, M. Daenen, K. Haenen, E. Ōsawa and M. Takahashi, *Chem. Phys. Lett.* **445**, 255 (2007).
- [10] M. P. Villar, M. P. Alegre, D. Araujo, É. Bustarret, P. Achatz, L. Saminadayar, C. Bäuerle and O. A. Williams, *Phys. Stat. Sol. (a)* **206**, 1986 (2009).
- [11] M. Bernard, A. Deneuve, T. Lagarde, É. Treboux, J. Pelletier, P. Muret, N. Casanova and É. Gheeraert, *Diamond and Related Materials* **11**, 828 (2002).
- [12] The asymmetry seen in the VI characteristics mainly arises due to an offset in our experimental setup, however, there is also a residual asymmetry which is presently not understood.
- [13] W. Rabaud, L. Saminadayar, D. Mailly, K. Hasselbach, A. Benoît and B. Étienne, *Phys. Rev. Lett.* **86**, 3124 (2001).
- [14] H. Courtois, M. Meschke, J. T. Peltonen and J. P. Pekola, *Phys. Rev. Lett.* **101**, 067002 (2008).
- [15] B. Sacépé, C. Chapelier, C. Marcenat, J. Kačmarčík, T. Klein, M. Bernard and É. Bustarret, *Phys. Rev. Lett.* **96**, 097006 (2006).
- [16] F. Dahlem, P. Achatz, O. A. Williams, D. Araujo, É. Bustarret and H. Courtois, *arXiv: Cond-Mat* 0912.3727v1 (2009).